A&A, 714, A357 (2026)
https://doi.org/10.1051/0004-6361/202662286
© The Authors 2026

Astronomy & Astrophysics

Nonzero phase shift of evanescent acoustic waves in the lower solar atmosphere

Hirdesh Kumar[1,2,⋆], S. P. Rajaguru[3], and Brajesh Kumar[4]

[1] Instituto de Astrofísica de Canarias, C/ Vía Láctea s/n, 38205 La Laguna, Tenerife, Spain
[2] Departamento de Astrofísica, Universidad de La Laguna, 38205 La Laguna, Tenerife, Spain
[3] Indian Institute of Astrophysics, Bangalore, India
[4] Udaipur Solar Observatory, Physical Research Laboratory, Udaipur, Rajasthan, India

Received 29 July 2026 / Accepted 2 September 2026

ABSTRACT

Context. The phase behavior of acoustic waves in the lower solar atmosphere provides important information about wave propagation. While previous studies have reported nonzero phase shifts in the evanescent frequency range and possible sign reversals near the frequency 3.0 mHz, the observational robustness and physical interpretation of these signatures remain uncertain.
Aims. We investigated the phase shifts and travel times of acoustic waves within the photosphere and across the photosphere–chromosphere interface in the quiet-Sun atmosphere and also assessed their height and frequency-dependent behavior.
Methods. Multi-height line-of-sight velocities were inferred using the bisector method applied to the photospheric Fe I 6173 Å and chromospheric Hα 6563 Å spectral lines observed with the Swedish Solar Telescope (SST). Fast Fourier transform analysis was employed to determine the phase shifts and travel times between the velocity signals derived at different bisector levels. In addition, k–ω phase-difference diagnostics were used to examine the wave number and frequency-dependent characteristics of wave propagation.
Results. Nonzero phase shifts are detected for acoustic waves in the evanescent frequency range within the photosphere, corresponding to phase travel times on the order of 1 s. In contrast to previous studies, no reversal in the sign of the phase shift or travel time is observed near 3 mHz in the Fe I 6173 Å observations. The measured phase shifts maintain the same sign throughout the investigated frequency range, suggesting the influence of complex wave dynamics. Measurements between velocities inferred from the Fe I and Hα lines exhibit a decrease in the 6–8 mHz frequency range. Our k–ω phase-difference analysis shows that this behavior is mainly caused by phase wrapping near 6.5 mHz rather than by an intrinsic change in wave propagation.
Conclusions. Our findings support the presence of nonzero phase differences within the evanescent frequency range while revealing discrepancies with earlier reports of phase-shift sign reversals near 3 mHz. We also highlight the importance of proper phase unwrapping for an accurate interpretation of acoustic-wave propagation in the lower solar atmosphere.

Key words. Sun: atmosphere – Sun: chromosphere – Sun: helioseismology – Sun: magnetic fields – Sun: oscillations – Sun: photosphere

1. Introduction

Time–distance analysis (Duvall et al. 1993) is widely used in local helioseismology to infer the travel times of acoustic waves traveling between different locations on the solar surface through the cross-correlation of oscillation signals. These waves are generated within the solar convection zone and propagate throughout the solar interior, where they are trapped in acoustic cavities, thereby forming standing waves that appear as ridges in the k–ω power spectrum (Ulrich 1970; Deubner 1975). Acoustic waves with frequencies up to ~5 mHz are generally evanescent, whereas higher-frequency acoustic waves can propagate freely through the quiet-Sun atmosphere. Measurements of acoustic travel times have been extensively used to investigate various subsurface solar phenomena, such as meridional flows (Giles et al. 1997; Chou & Dai 2001; Zhao & Kosovichev 2004; Zhao et al. 2012).

Utilizing time–distance analysis, Zhao et al. (2012) reported a systematic center-to-limb variation in helioseismic travel times derived from observations obtained with the Helioseismic and Magnetic Imager (HMI; Scherrer et al. (2012); Schou et al. 2012) instrument on board the Solar Dynamics Observatory (SDO; Pesnell et al. 2012) spacecraft. They suggested that the effect could be due to the line formation height of the spectral line used for the observations and that it should be properly accounted for when inferring internal meridional flows. Subsequently, Zhao et al. (2016) showed that foreshortening effects are not responsible for the observed center-to-limb variation in acoustic travel-time differences, which are crucial for accurate measurements of meridional circulation. Using Doppler velocity observations from HMI/SDO, Chen & Zhao (2018) investigated the center-to-limb effect in the frequency domain and examined its dependence on solar disk position, travel distance, and wave frequency. Their analysis reveals a strong frequency dependence of the ceneter to limb (CtoL) effect, including a sign reversal near 5.4 mHz close to the disk center and a maximum amplitude around 4.0 mHz prior to the reversal. In contrast, the flow-induced travel-time shifts did not exhibit significant frequency dependence.

Using multi-height line-of-sight (LOS) velocities derived through the bisector method applied to the Fe I 6173 Å observations acquired with the Interferometric BIdimensional Spectrometer (IBIS; Cavallini 2006) instrument installed at the Dunn Solar Telescope (DST), Zhao et al. (2022) report the

⋆ Corresponding author: hirdeshchauhan71@gmail.com

Open Access article, published by EDP Sciences, under the terms of the Creative Commons Attribution License (https://creativecommons.org/licenses/by/4.0), which permits unrestricted use, distribution, and reproduction in any medium, provided the original work is properly cited.
This article is published in open access under the Subscribe to Open model. Subscribe to A&A to support open access publication.

non-evanescent behavior of evanescent acoustic waves in the quiet photosphere. Although the observed field of view (FOV) contains a small sunspot near the center, the quiet region analyzed was selected from the surrounding weakly magnetized area. Their study reveals phase-travel-time variations with amplitudes of approximately 1 s up to 5 mHz for velocity–velocity pairs derived from different heights within the Fe I line. They also detect a sign reversal in both phase-shift and travel-time measurements around 3 mHz. This non-evanescent behavior was interpreted as a combined effect of atmospheric non-adiabaticity and asymmetry in the Fe I 6173 Å spectral profile. However, the influence of surrounding magnetic fields remained a potential concern for the measured phase shifts. Further, Waidele et al. (2023) estimated phase shifts and travel times of acoustic waves using synthetic Fe I 6173 Å observations generated from fully radiative and convective atmospheric simulations. Their analysis also demonstrates the non-evanescent behavior of evanescent acoustic waves. Importantly, they report substantial differences between phase shifts derived from true velocities and those inferred from synthetic spectral observations. In particular, the sign reversal in phase shift occurred near 4.0 mHz in the true-velocity analysis. Based on these discrepancies, they concluded that nonadiabatic atmospheric effects introduce additional phase shifts.

More recently, Kumar et al. (2024) investigated acoustic-wave phase shifts in the quiet-Sun atmosphere using Fe I 6173 Å and Ca II 8542 Å line-scan observations obtained with the Narrow Band Imager (NBI; Mathew et al. (2017)) instrument installed at the Multi-Application Solar Telescope (MAST; Venkatakrishnan et al. 2017) operational at the Udaipur Solar Observatory in Udaipur, India. By applying the bisector method to the Fe I 6173 Å and Ca II 8542 Å spectral profiles at different line-depth positions, they derived multi-height LOS velocities. Their analysis of phase shifts and travel times in regions with LOS magnetic fields below 10 G again demonstrate the non-evanescent behavior of evanescent acoustic waves. They also report a sign reversal in phase shift and travel times around 3.0 mHz, supporting the interpretation that atmospheric non-adiabaticity and spectral-line asymmetry are responsible for this behavior. Their results further suggest that the effect is independent of the specific instrument used for Fe I 6173 Å observations. Additionally, the phase shifts measured from photospheric and chromospheric multi-height velocities exhibited a roll-off beginning near 6 mHz (Kumar et al. 2024). A similar roll-off across the photosphere–lower-chromosphere interface is also reported by Chaturmutha et al. (2024) in phase-travel measurements of acoustic-waves, limiting the applicability of simple two-wave models for travel-time interpretation. However, the physical origin of this roll-off remains poorly understood.

In this article, we revisit and analyze the phase shifts of acoustic waves in a quiet-Sun region, both within the photosphere and across the photosphere–chromosphere interface. Our analysis uses high-spatial-resolution observations in the Fe I 6173 Å and Hα 6563 Å spectral lines, acquired with the 1-m Swedish Solar Telescope (SST; Scharmer et al. 2003) at La Palma. A distinctive feature of these observations is that the entire solar disk was free of detectable magnetic structures during the observing period. This contrasts with the quiet-Sun datasets analyzed by Kumar et al. (2024) and Zhao et al. (2022), where strong magnetic structures were present in the immediate neighborhood. Acoustic waves with large horizontal wavelengths can originate outside the observed FOV, and their propagation may be influenced by magnetic fields encountered along their paths. Consequently, the absence of magnetic structures across the entire solar disk during our observations minimizes the possibility that the measured wave properties are affected by magnetic fields originating outside the observed FOV. The inclusion of Hα observations, which sample higher atmospheric layers than the Fe I 6173 Å line, enables a more comprehensive investigation of the previously reported roll-off in acoustic-wave phase shifts and travel times. The article is organized as follows. Section 2 describes the observations and analysis methods; Sect. 3 presents the results; and Sect. 4 discusses the implications of our findings.

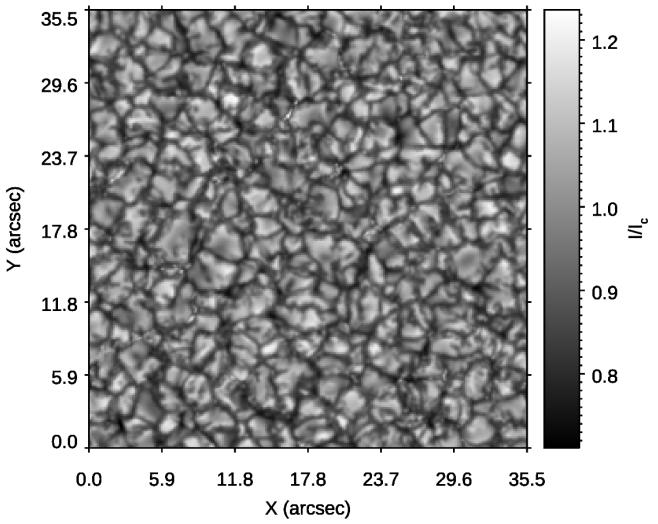


Fig. 1. Photospheric continuum intensity map illustrating the region of interest used in our analysis corresponding to the start time of the observations.

2. Observations and data analysis

2.1. SST observations

We utilized quiet-Sun observations obtained at the solar disk center on 24 April 2019 with the SST. The observations span 08:30–10:30 UT, with a cadence of 28.18 s and a pixel size of 0.0591 arcsec. Photospheric observations were acquired in the Fe I 6173 Å spectral line at 15 wavelength positions with a sampling of 35 mÅ. For chromospheric diagnostics, the Hα and Ca II 8542 Å lines were observed at 25 and 20 wavelength positions, respectively, using the CRisp Imaging Spectropolarimeter (CRISP; Scharmer et al. 2008). The observations were performed using the adaptive optics system installed at the SST (Scharmer et al. 2019) and were subsequently corrected using the Multi-Object Multi-Frame Blind Deconvolution (MOMFBD; Van Noort et al. 2005) technique. Figure 1 presents the photospheric continuum intensity image from the Fe I observations, selected from the CRISP/SST FOV for our analysis.

2.2. Velocity-velocity phase shift and phase travel time analysis

Multi-height LOS velocities were estimated using the bisector method (Gray 2005). This method is widely employed to derive LOS velocities at different intensity levels within spectral lines (Kumar et al. 2024). It is particularly effective in the quiet-Sun region, where the spectral line profiles generally retain a regular shape and thereby provide robust measurements of LOS

velocities. Here, we used only the Fe I and Hα spectral lines to probe the photosphere and the photosphere–chromosphere interface regions of the solar atmosphere. The Ca II line was excluded from our velocity analysis because the line core exhibits emission features at certain locations in the presence of background magnetic fields, which complicates reliable velocity estimation. In addition, the core of the Hα line probe higher layers of the chromosphere than the core of Ca II 8542 Å line. The bisector method was applied at 10% intensity intervals in the Fe I line, where PV0 corresponds to the line-core velocity and PV7 represents the velocity near the line wings (see the left panel of Fig. 2). Similarly, for the Hα line, CV0 denotes the line-core velocity, and CV7 corresponds to the velocity near the line wings (see the right panel of Fig. 2). The continuum of the Fe I line is assumed to form at a height of approximately 20 km above $\tau = 1$ at 500 nm, while its line core samples heights around 300 km in the quiet-Sun atmosphere (Norton et al. 2006). The H(α) core is sensitive to the middle chromosphere, whereas its wings probe regions near the temperature minimum (Vernazza et al. 1973, 1976, 1981). Therefore, the velocities inferred from the bisector analysis of the Fe I and Hα lines, spanning from PV7 to PV0 and from CV7 to CV0, respectively, provide multi-height LOS velocity measurements across different layers of the solar atmosphere. It should be noted that the bisector velocities are not generated from thin atmospheric layers within the line-forming height in the solar atmosphere; therefore, the analysis presented here shows the average phase and coherence estimated over full FOV from velocity–velocity pairs.

We estimated the cross-spectra between the pairs of velocity signals obtained at different bisector levels to derive the phase difference ($\delta\phi(\nu)$) and phase travel times ($t_{ph}(\nu)$) of waves as a function of frequency (ν). The two-height cross-spectra were computed from temporal velocity signals measured at different bisector levels. These quantities were evaluated independently at each spatial location (pixel) within the FOV. Thus, the derived quantities form spatially resolved maps, denoted as tph(x, y, ν), where x and y represent the spatial coordinates and ν is the temporal frequency.

For the two time series, $I_1(t)$ and $I_2(t)$, the complex cross-spectrum is defined as the product of the Fourier transform of one signal and the complex conjugate of the Fourier transform of the other signal:

$$X_{12}(\nu) = I_1(\nu) \times I_2^*(\nu), \tag{1}$$

where $I_1(\nu)$ and $I_2^*(\nu)$ are the Fourier transforms of the corresponding time series and the superscript (*) denotes complex conjugation.

The phase lag, $\delta\phi(\nu)$, between the two signals was obtained from the argument (phase angle) of the complex cross-spectrum:

$$\delta\phi(\nu) = \tan^{-1}\left[\frac{\mathrm{Im}\,(X_{12}(\nu))}{\mathrm{Re}\,(X_{12}(\nu))}\right], \tag{2}$$

where Re and Im denote the real and imaginary parts of the cross-spectrum, respectively.

The magnitude of the cross-spectrum was further used to compute the coherence (C) between the two signals, which quantifies the degree of linear correlation as a function of frequency:

$$C(\nu) = \frac{|\langle X_{12}(\nu)\rangle|^2}{\left\langle |I_1(\nu)|^2\right\rangle \left\langle |I_2(\nu)|^2\right\rangle}. \tag{3}$$

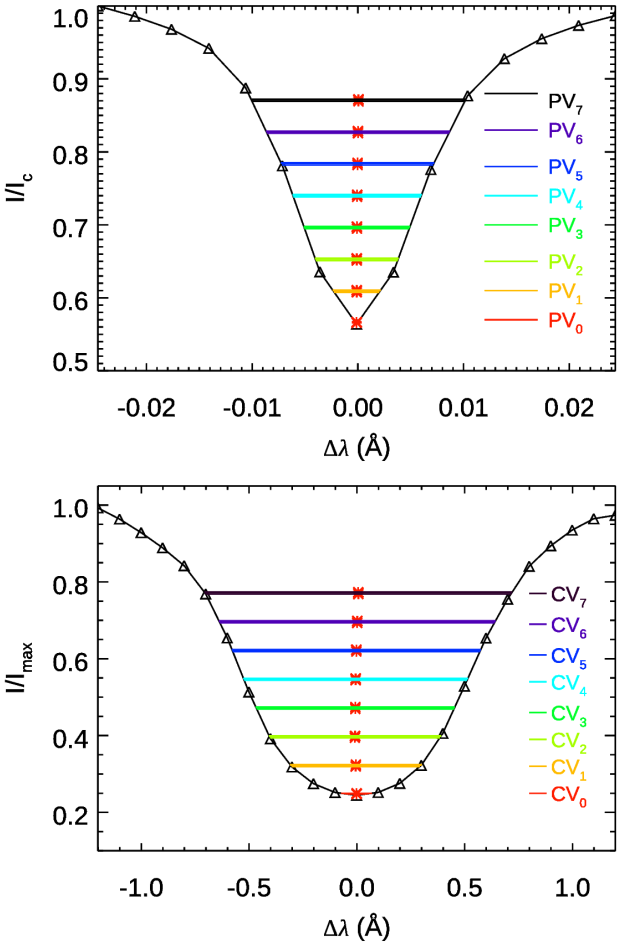


Fig. 2. Photospheric Fe I (top panel) and chromospheric Hα (bottom panel) spectral profiles obtained from the average intensity over the full FOV, as shown in Fig. 1, showing the bisector at 10% line-depth intensity intervals, respectively.

The coherence ranges between 0 and 1. Values close to 1 indicate a strong and stable phase relationship between the two time series at a given frequency, whereas values close to 0 imply little or poor correlation.

The phase travel time, $t_{\mathrm{ph}}(\nu)$, is defined as the temporal lag corresponding to the phase difference $\delta\phi(\nu)$,

$$t_{\mathrm{ph}}(\nu) = \frac{\delta\phi(\nu)}{2\pi\nu}. \tag{4}$$

In our sign convention, positive values of $\delta\phi(\nu)$ and $t_{\mathrm{ph}}(\nu)$ indicate upward wave propagation (i.e., the wave propagates from photosphere to chromosphere), whereas negative values correspond to downward propagation.

The estimated $\delta\phi(\nu)$ and $t_{\mathrm{ph}}(\nu)$ values derived from photospheric and chromospheric velocity or intensity observations also contain contributions from solar atmospheric gravity waves. These waves occupy the low-frequency region below the f-mode (surface gravity wave) ridge in the k–ω dispersion diagram (Straus et al. 2008). Although these gravity waves transport energy upward, from the photosphere to the chromosphere, they exhibit negative phase differences.

As our primary interest is the propagation of acoustic waves, we first applied a 3D Fourier filter in (k_x, k_y, ν) space to the velocity data cubes obtained at different bisector levels. The

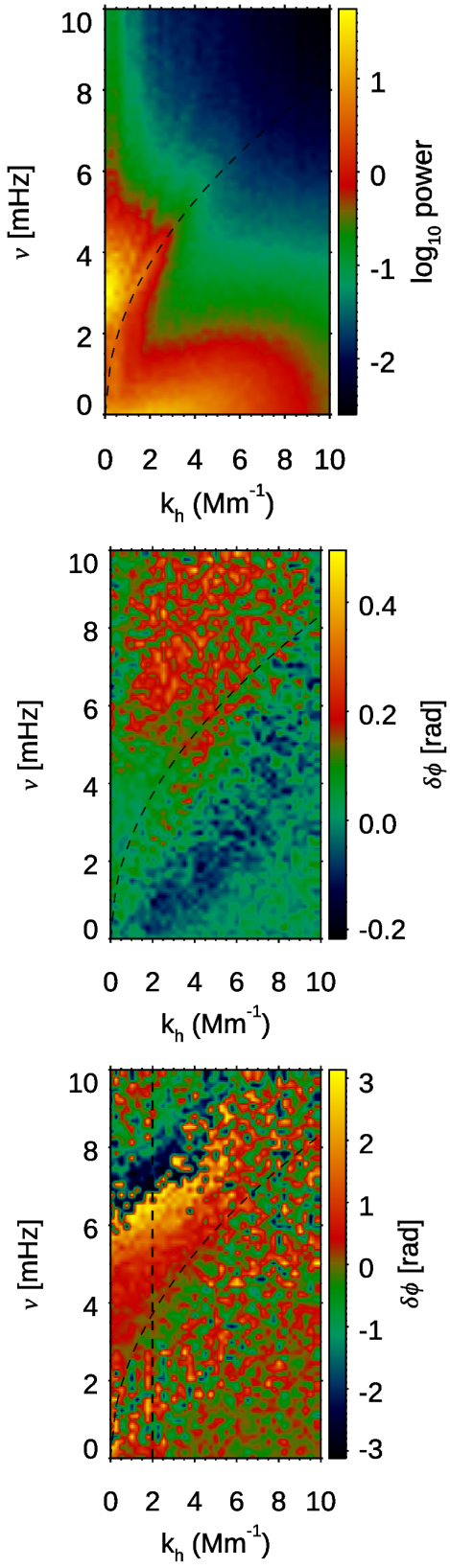


Fig. 3. *Left panel*: photospheric power diagnostic diagram constructed from the PV7 velocity data cubes. *Middle panel*: phase difference diagnostic diagram obtained from the PV7 – PV0 photospheric velocity pair. *Right panel*: same as middle panel but for the photospheric PV7 and Chromospheric CV3 velocity pairs. The slanted dashed black line represents the f mode.

filter was designed to suppress contributions from the surface-gravity (f) modes and atmospheric gravity waves prior to the cross-spectral analysis described above. Following the approach of Giles (2000) and Rajaguru et al. (2004), the locations of the f and $p1$ mode ridges in the $k-\omega$ diagram were used to define the filtering boundaries. We suppressed the region below the $p1$ mode ridge using a Gaussian filter, which progressively attenuates the power well below the $p1$ mode and thereby removes the dominant f mode and atmospheric gravity-wave contribution. The resulting filtered velocity cubes were then used for the cross-spectral analysis of the phase differences and travel times.

The top panel of Fig. 3 shows the k–ω power diagnostic diagram constructed from the PV7 velocity data cube. The diagram was obtained by applying a fast Fourier transform (FFT) to the velocity cube and subsequently azimuthally averaging over k_x and k_y. The ridges observed in the k–ω diagram correspond to acoustic waves trapped within the solar interior, forming standing waves that appear as characteristic ridges in the power spectrum. The overplotted dashed curve marks the location of the f mode. Below the f-mode ridge, the power is dominated by atmospheric gravity waves and convective noise. The middle panel of Fig. 3 presents the k–ω phase-difference diagram derived from the PV7–PV0 velocity pair, corresponding to measurements within the photosphere. A positive phase shift above the f mode indicates the well-known upward propagation of high-frequency acoustic waves. In contrast, below the f-mode ridge, the atmospheric gravity waves are clearly visible through their characteristic negative phase shifts (Straus et al. 2008; Kumar et al. 2023). The bottom panel of Fig. 3 shows the phase-difference diagram between the photospheric velocity (PV7) and chromospheric velocity (CV3). In this case, positive phase shifts are observed above the f mode, corresponding to acoustic-wave propagation. However, a negative phase shift appears in the 6–8 mHz frequency range. We discuss this feature in detail in Sect. 4. The phase shift, $\delta\phi(\nu)$, of acoustic waves, computed over the full FOV and subsequently spatially averaged, is shown as a function of frequency, ν in the top panel of Fig. 4 for the various velocity pairs indicated. The corresponding phase travel time, $t_{\rm ph}(\nu)$, is presented in the middle panel of Fig. 4, while the bottom panel shows the coherence estimated between two height velocity–velocity pairs used to obtain the phase difference and travel time. We can clearly see that coherence is significantly high and highlight that, as the height difference between the two velocity–velocity pairs increases, coherence decreases. It is generally expected that, as waves travel to greater heights, they lose coherence. Figure 5 further displays the phase shifts, phase travel times, and coherence derived from different photospheric (PV7) and chromospheric (CV0) velocity pairs, averaged over the entire FOV.

3. Results

3.1. Phase shift and phase travel time within the photosphere

In this particular observational dataset, the measured phase shifts ($\delta\phi(\nu)$), and the corresponding phase travel times ($t_{\rm ph}(\nu)$), derived from different bisector driven velocity–velocity pairs within the photosphere (Fig. 4) provide important insights into the propagation characteristics of acoustic waves in the lower solar atmosphere. The inferred phase relationships reveal clear signatures of wave propagation across the sampled photospheric layers and demonstrate dependency of the phase on both frequency and atmospheric height separation. High coherence

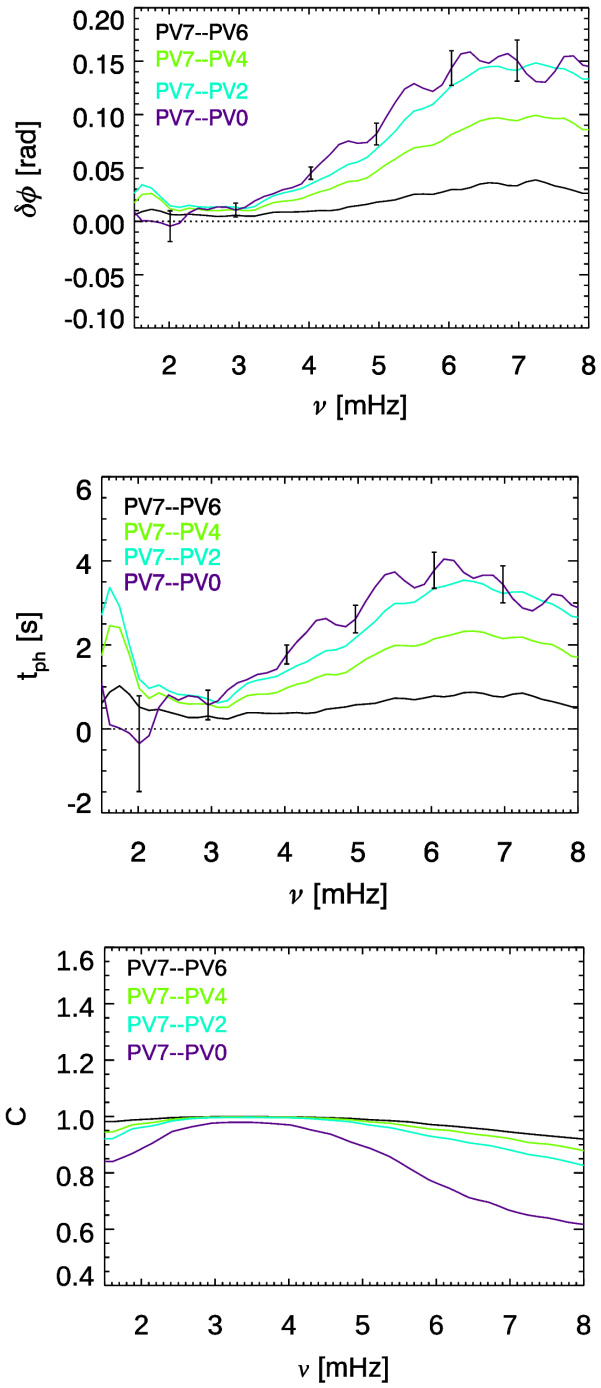


Fig. 4. Phase shift (*top panel*), phase travel time (*middle panel*), and coherence (*bottom panel*) of acoustic waves derived from different velocity–velocity pairs, as indicated in the plots, within the photosphere as a function of frequency. For clarity, standard errors are displayed only for selected points in one of these curves, and the errors for the other points in this and in other curves are similar. The coherence panel corresponds to the same velocity pairs used for estimating the phase difference and phase travel times of the acoustic waves.

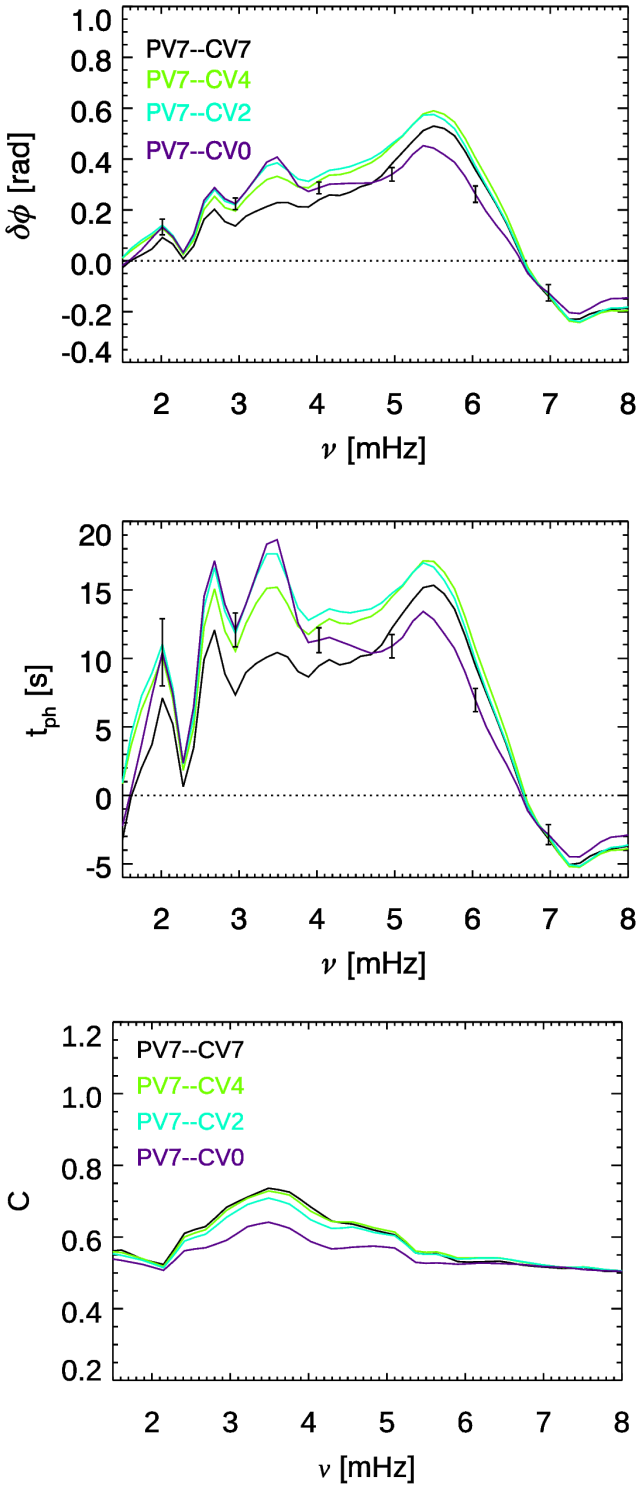


Fig. 5. Same as Fig. 4 but for photospheric-chromospheric velocity pairs.

values are observed across the frequency range and for all velocity pairs, indicating a strong correlation between the velocity signals (see bottom panel of Fig. 4). To ensure the reliability of the phase measurements, we restricted our physical interpretation to frequency ranges where the coherence (C), exceeds 0.5. Phase differences at frequencies with C < 0.5 were excluded from the interpretation because phase estimates become increasingly uncertain as coherence decreases. Thus, the phase differences discussed here correspond to frequency ranges in which the two velocity signals satisfy the adopted coherence criterion (C > 0.5) and were therefore retained for interpretation. At frequencies below approximately 5 mHz, the observed phase shifts remain relatively small, while the corresponding phase travel times are on the order of ∼1 s. These results indicate that

the waves in this evanescent acoustic frequency regime exhibit nearly non-evanescent behavior within the photosphere, consistent with earlier observational investigations of photospheric acoustic-wave propagation (Zhao et al. 2022; Kumar et al. 2024). In contrast, the high-frequency ($\nu > 5.0$ mHz) acoustic waves display the characteristic quiet-Sun behavior commonly reported in previous studies. Specifically, the phase difference increases progressively with frequency, indicating more efficient upward propagation of acoustic waves at higher frequencies. This is consistent with the expectation that waves with frequencies above the acoustic cut-off are less affected by atmospheric stratification and therefore propagate more freely through the photospheric layers and dissipate energy in the higher solar atmosphere through shock formation. We further note that the measured phase difference, $\delta\phi(\nu)$, is not determined solely by the temporal frequency, ν, but also depends strongly on the separation between the atmospheric layers sampled by the velocity signals. Among the analyzed velocity pairs, the PV7–PV0 pair spans the largest separation within the formation region of the Fe I spectral line and consequently exhibits the largest phase shifts over the investigated frequency range. In comparison, velocity pairs with smaller separations show systematically reduced phase differences and shorter travel times. This behavior is physically expected, since acoustic waves propagating through a larger vertical distance accumulate a correspondingly larger phase delay. The observed dependence of $\delta\phi(\nu)$ on the separation between the sampled atmospheric layers is, therefore, consistent with the interpretation that the measured phase signatures are primarily associated with vertically propagating acoustic disturbances within the photosphere.

3.2. Phase shift and phase travel time within the photosphere-chromosphere interface

Figure 5 reveals a striking systematic behavior in the variation of the phase shift ($\delta\phi(\nu)$) and phase travel time ($t_{\rm ph}(\nu)$), across the photosphere–chromosphere interface. The derived phase diagnostics from all photospheric–chromospheric velocity pairs exhibit a broadly similar frequency dependence, indicating the presence of common physical processes governing wave propagation between these atmospheric layers. At lower frequencies, up to approximately 5.5 mHz, both the phase shifts and the corresponding phase travel times display significant fluctuations with frequency, with higher coherence (C > 0.5) between all velocities pairs (bottom panel of Fig. 5). In this regime, the measured phase differences remain predominantly positive, suggesting the upward propagation of acoustic waves from the photosphere toward the chromosphere. Beyond frequencies of approximately 5.5 mHz, the phase behavior undergoes a pronounced roll-off, characterized by a rapid decrease in the measured phase shifts and phase travel times. This decline ultimately leads to negative phase shifts near ~6.5 mHz for nearly all velocity pairs. The transition from positive to negative phase differences represents a significant change in the wave-propagation characteristics across the photosphere–chromosphere interface and indicates that the high-frequency waves cannot be interpreted solely in terms of simple upwardly propagating acoustic waves.

Similar to the behavior observed for photospheric velocity pairs, we find that both $\delta\phi(\nu)$ and $t_{\rm ph}(\nu)$ depend not only on frequency but also on the separation between the two sampled atmospheric layers. In general, velocity pairs covering the largest separation exhibit stronger phase variations and longer travel times, consistent with the expectation that waves propagating through greater vertical distances accumulate larger phase delays. However, the PV7–CV0 pair deviates from this general trend, suggesting that additional physical effects or local variability in the chromosphere may influence the measured phase relationship for this particular combination of atmospheric heights. A comparable high-frequency roll-off and transition toward negative phase shifts has previously been reported in both velocity–velocity and intensity–intensity measurements probing the photosphere–chromosphere layers of the solar atmosphere (Zhao et al. 2022; Chaturmutha et al. 2024; Kumar et al. 2024). The observed roll-off poses important challenges for the theoretical and numerical models attempting to accurately describe wave propagation across the photosphere–chromosphere interface (Chaturmutha et al. 2024). The physical origin of the observed roll-off and its implications for chromospheric wave propagation are examined in detail in the following section.

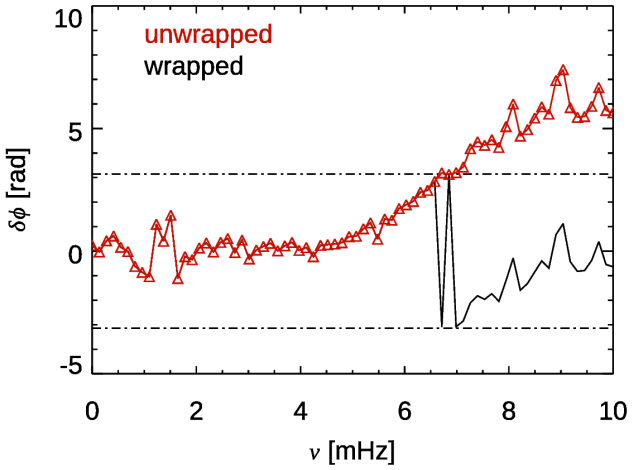


Fig. 6. Phase shift as a function of frequency at a fixed wave number ($k_h = 2$ M m^{-1}) obtained from the photospheric PV7 and chromospheric CV3, k-ω diagram, as highlighted in the bottom panel of Fig. 3 with the vertical dashed black line. The black plot shows the wrapped phase shift, highlighting the wrapping around 6.5 mHz. The overplotted red curve shows the unwrapped phase shift.

4. Discussions and conclusions

In this study, we examined the phase shifts and phase travel times of acoustic waves within the photosphere and across the photosphere–chromosphere interface using multi-height Doppler velocities derived from bisector analysis of the photospheric Fe I 6173 Å and chromospheric Hα spectral lines observed with the SST. The use of multi-height velocity measurements allowed us to examine the frequency- and wavenumber-dependent propagation of acoustic waves over a wide range of atmospheric layers in the quiet Sun. We used Fourier cross-spectral and $k-\omega$ diagnostic techniques to measure the phase behavior. The cross-spectral analysis determines the frequency-dependent phase difference between the two velocity signals and is, therefore, useful for quantifying the frequency-dependent phase variation and associated time delay. However, because this analysis is spatially averaged, it does not retain explicit information about the horizontal wave number of the waves. In particular, phase values approaching $\pm\pi$ may lead to an apparent change in the sign of the measured phase owing to phase wrapping. The $k-\omega$ analysis provides the additional spatial-frequency information required to examine this behavior.

The combination of the two diagnostics thus allows us to distinguish the frequency-dependent phase relation from an apparent phase reversal caused by phase wrapping.

Our analysis confirms the presence of nonzero phase shifts and finite phase travel times for low-frequency acoustic waves within the photosphere. In the frequency range below the acoustic cut-off frequency ($\nu \lesssim 5$ mHz), where acoustic waves are generally expected to behave as evanescent waves, we still detect small but systematic positive phase lags between velocity signals formed at different heights. Similar non-evanescent behavior of low-frequency acoustic waves has previously been reported by Zhao et al. (2022), Waidele et al. (2023) and Kumar et al. (2024). Using Fe I 6173 Å and Ca II 8542 Å observations from the NBI/MAST instrument, Kumar et al. (2024), in particular, show that these nonzero phase shifts remain even after limiting the analysis to regions with LOS magnetic fields below 10 G, thereby reducing possible magnetic effects. Our SST observations independently confirm these findings and provide further evidence that low-frequency acoustic waves in the quiet-Sun photosphere can exhibit measurable upward phase propagation. However, an important difference emerges when our results are compared with previous observational studies. Both Zhao et al. (2022) and Kumar et al. (2024) report a reversal in the sign of the phase shift and phase travel time near ∼3 mHz within the photosphere. In contrast, our SST observations do not show such a sign reversal (Fig. 4). Instead, the measured phase shifts remain predominantly positive throughout the low-frequency regime, indicating a persistent upward phase propagation. Using 3D radiation-hydrodynamic simulations, Waidele et al. (2023) synthesized the Fe I 6173 Å spectral line and derived Doppler velocities at different intensity levels within the line profile. Their analysis of velocities inferred from the synthesized spectra do not reveal a sign reversal at $\nu \approx 3$ mHz (see Fig. 8 a, (Waidele et al. 2023)). The agreement between our observations and the results obtained from synthetic velocity therefore raises questions about the physical origin of the 3 mHz sign reversal reported in earlier observational studies. This discrepancy suggests that the phase behavior of the low-frequency acoustic waves in the lower solar atmosphere may be more complex than previously inferred from observations alone.

It is worth noting that the quiet-Sun observations used for the phase-shift analysis by Zhao et al. (2022) and Kumar et al. (2024) were obtained in regions located in the vicinity of strong magnetic structures, with several active regions also present on the solar disk (see panels a and b of Fig. 7). These panels show the photospheric LOS magnetograms obtained from the Michelson Doppler Imager (MDI; Scherrer et al. 1995) on board the Solar and Heliospheric Observatory (SOHO; Domingo et al. 1995) and the Helioseismic and Magnetic Imager (HMI; Scherrer et al. 2012) on board the Solar Dynamics Observatory (SDO; Pesnell et al. 2012), respectively. For visualization, the magnetograms were saturated at ±100 G to enhance the visibility of small-scale magnetic structures. Acoustic waves with relatively large horizontal wavelengths originating outside the observed FOV may therefore encounter magnetic structures before reaching the region sampled by the observations, potentially influencing their phase behavior even when the observed region itself appears relatively quiet. In contrast, our observations were obtained from a region of the solar disk in which no detectable strong magnetic concentrations are apparent in the co-temporal HMI LOS magnetogram (Fig. 7c). The magnetogram is displayed with the same ±100 G saturation limits, and no distinct magnetic structures are visible within the observed region at this level. We emphasize that this criterion does not imply the complete absence of magnetic fields. Rather, it identifies a region without detectable strong magnetic concentrations at the spatial resolution and sensitivity of the magnetogram. Thus, the contribution of strong magnetic structures to the measured phase behavior is expected to be comparatively small in our observations. This difference

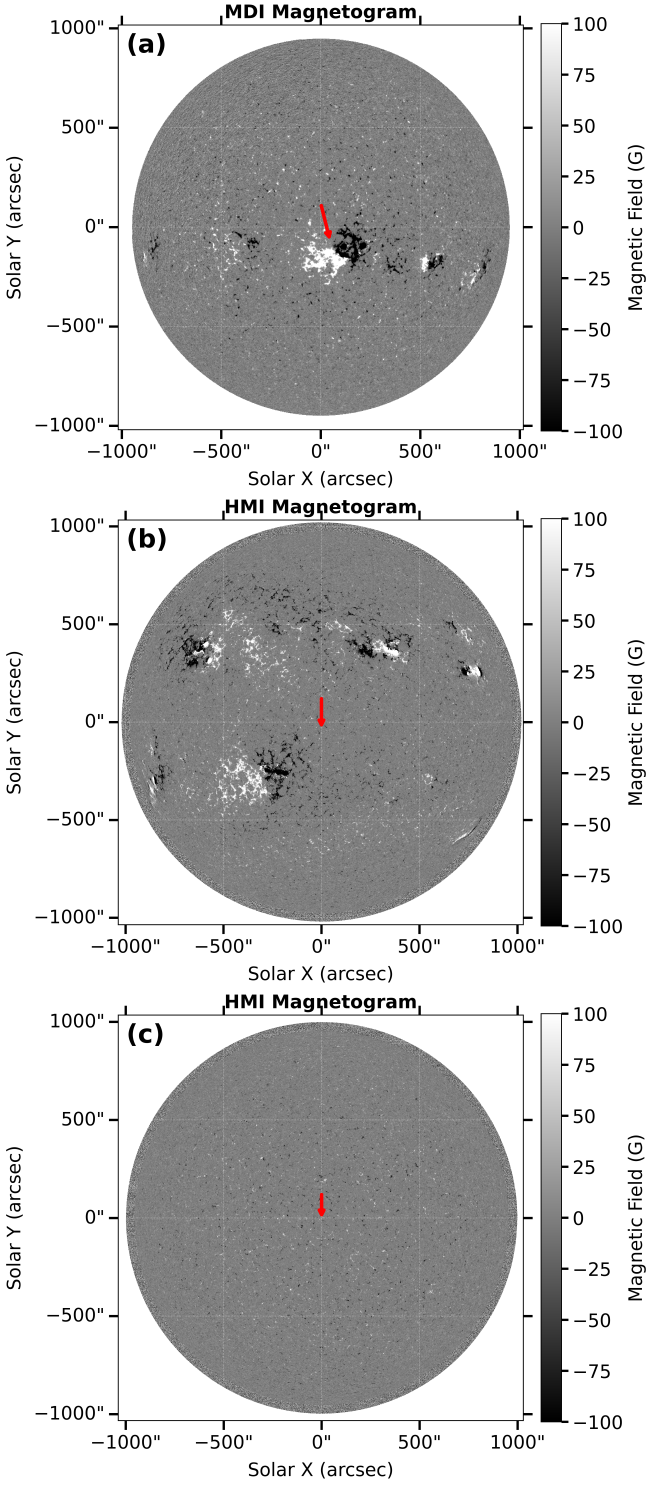


Fig. 7. Sample photospheric magnetograms corresponding to the date of observations used in the previous analysis performed by Zhao et al. (2022) (panel a) and Kumar et al. (2024) (panel b). Panel c: date of the observations used in this study. The red arrowhead indicates the approximate position of the quiet-Sun region selected for the analysis.

in the magnetic environment may be one possible factor contributing to the absence of the phase-sign reversal near 3 mHz found in some previous studies. However, we cannot exclude other factors, such as differences in instrumental characteristics, spectral sampling, velocity-extraction techniques, spatial resolution, and the formation and response of the spectral lines. We thus regard the magnetic environment as a possible contributing factor rather than a unique explanation for the different phase behavior observed near 3 mHz. Additional observational and numerical investigations are therefore be required to determine whether the previously reported sign reversal represents a genuine physical phenomenon or arises from observational and diagnostic effects associated with velocity measurements in the solar photosphere. At higher frequencies ($\nu > 5$ mHz), the observed phase shifts increase steadily with frequency, consistent with the expected upward propagation of acoustic waves above the acoustic cut-off frequency. This behavior agrees with the standard quiet-Sun picture, where high-frequency acoustic waves propagate more freely through the stratified atmosphere and may dissipate energy in the upper atmosphere through shock formation. The increase in phase difference with increasing height separation between velocity pairs further supports the interpretation that the measured phase signals are dominated by vertically propagating acoustic waves.

Across the photosphere–chromosphere interface, the phase shifts show much more complex behavior. While the phase differences remain mostly positive below ~5.5 mHz, all velocity pairs show a strong decrease in phase shift at higher frequencies, eventually becoming negative near ~6.5 mHz. Similar high-frequency roll-off behavior has previously been reported in both velocity–velocity and intensity–intensity measurements across the photosphere–chromosphere interface (Zhao et al. 2022; Chaturmutha et al. 2024; Kumar et al. 2024). This observed roll-off has been a major challenge for theoretical models of acoustic-wave propagation in the lower solar atmosphere. To understand the origin of this behavior, we examined the k–ω phase-difference diagram derived from the PV7–CV3 velocity pair. The analysis shows clear evidence of phase wrapping in the 6–8 mHz frequency range. This becomes especially clear when examining the phase variation at a fixed horizontal wave number of $k_h = 2$ M m^{-1} (Fig. 6). The wrapped phase appears to change signs near 6.5 mHz, whereas the unwrapped phase remains continuous. This demonstrates that the observed roll-off in the spatially averaged phase shifts and travel times is mainly caused by phase wrapping rather than by an actual reversal in wave propagation. The effect of phase wrapping is partly smoothed out when averaging over the full FOV, producing an apparent roll-off in the mean phase curves. Our results therefore show that phase wrapping must be carefully examined before spatial averaging is performed, especially when comparing observations with theoretical wave-propagation models, such as those proposed by Chaturmutha et al. (2024). Ignoring phase wrapping may lead to incorrect interpretations of wave travel times and propagation properties across the photosphere–chromosphere interface.

In conclusion, our analysis confirms the presence of nonzero phase shifts and finite phase travel times for low-frequency acoustic waves in the quiet-Sun photosphere. The observed phase shift may include contributions from several effects, including radiative losses or non-adiabaticity, spectral-line response functions, height-dependent velocity response, and atmospheric dynamics, which modify the behavior of acoustic waves in the evanescent frequency range. While we confirm the existence of nonzero phase shifts, we do not detect the previously reported phase-sign reversal near 3 mHz. Instead, the phase shifts remain predominantly positive, consistent with recent radiation-hydrodynamic simulations. In addition, the apparent high-frequency roll-off observed across the photosphere–chromosphere interface is found to be largely caused by phase wrapping rather than by an intrinsic change in wave propagation. These findings highlight the importance of accounting for physical and diagnostic effects and phase wrapping when interpreting acoustic-wave propagation in the lower solar atmosphere.

Acknowledgements. We thank the referee for his/her constructive suggestions, which improved the presentation of our results. The 1-m Swedish Solar Telescope is operated on the island of La Palma by the Institute for Solar Physics of Stockholm University in the Spanish Observatorio del Roque de los Muchachos of the Instituto de Astrofísica de Canarias. H.K. acknowledge funding from grant CNS2023-145233 funded by MICIU/AEI/10.13039/501100011033 and by "European Union NextGenerationEU/PRTR". The work of S.P. Rajaguru and Brajesh Kumar are supported by Department of Science and Technology and Department of Space, Govt. of India, respectively.

References

Cavallini, F. 2006, Sol. Phys., 236, 415
Chaturmutha, V., Fleck, B., & Jefferies, S. M. 2024, ApJ, 966, 200
Chen, R., & Zhao, J. 2018, ApJ, 853, 161
Chou, D.-Y., & Dai, D.-C. 2001, ApJ, 559, L175
Deubner, F.-L. 1975, A&A, 44, 371
Domingo, V., Fleck, B., & Poland, A. I. 1995, Sol. Phys., 162, 1
Duvall, Jr., T. L., Jefferies, S. M., Harvey, J. W., & Pomerantz, M. A. 1993, Nature, 362, 430
Giles, P. M. 2000, PhD thesis, Stanford University, California
Giles, P. M., Duvall, T. L., Scherrer, P. H., & Bogart, R. S. 1997, Nature, 390, 52
Gray, D. F. 2005, The Observation and Analysis of Stellar Photospheres
Kumar, H., Kumar, B., & Rajaguru, S. P. 2023, Adv. Space Res., 72, 1898
Kumar, H., Kumar, B., Mathew, S. K., Bayanna, A. R., & Rajaguru, S. P. 2024, ApJ, 972, 39
Mathew, S. K., Bayanna, A. R., Tiwary, A. R., Bireddy, R., & Venkatakrishnan, P. 2017, Sol. Phys., 292, 106
Norton, A. A., Graham, J. P., Ulrich, R. K., et al. 2006, Sol. Phys., 239, 69
Pesnell, W. D., Thompson, B. J., & Chamberlin, P. C. 2012, Sol. Phys., 275, 3
Rajaguru, S. P., Hughes, S. J., & Thompson, M. J. 2004, Sol. Phys., 220, 381
Scharmer, G. B., Bjelksjo, K., Korhonen, T. K., Lindberg, B., & Petterson, B. 2003, SPIE Conf. Ser., 4853, 341
Scharmer, G. B., Narayan, G., Hillberg, T., et al. 2008, ApJ, 689, L69
Scharmer, G. B., Löfdahl, M. G., Sliepen, G., & de la Cruz Rodríguez, J. 2019, A&A, 626, A55
Scherrer, P. H., Bogart, R. S., Bush, R. I., et al. 1995, Sol. Phys., 162, 129
Scherrer, P. H., Schou, J., Bush, R. I., et al. 2012, Sol. Phys., 275, 207
Schou, J., Scherrer, P. H., Bush, R. I., et al. 2012, Sol. Phys., 275, 229
Straus, T., Fleck, B., Jefferies, S. M., et al. 2008, ApJ, 681, L125
Ulrich, R. K. 1970, ApJ, 162, 993
Van Noort, M., Rouppe Van Der Voort, L., & Löfdahl, M. G. 2005, Sol. Phys., 228, 191
Venkatakrishnan, P., Mathew, S. K., Srivastava, N., et al. 2017, Curr. Sci., 113, 686
Vernazza, J. E., Avrett, E. H., & Loeser, R. 1973, ApJ, 184, 605
Vernazza, J. E., Avrett, E. H., & Loeser, R. 1976, ApJS, 30, 1
Vernazza, J. E., Avrett, E. H., & Loeser, R. 1981, ApJS, 45, 635
Waidele, M., Zhao, J., & Kitiashvili, I. N. 2023, ApJ, 949, 99
Zhao, J., & Kosovichev, A. G. 2004, ApJ, 603, 776
Zhao, J., Nagashima, K., Bogart, R. S., Kosovichev, A. G., & Duvall, Jr., T. L. 2012, ApJ, 749, L5
Zhao, J., Stejko, A., & Chen, R. 2016, Sol. Phys., 291, 731
Zhao, J., Rajaguru, S. P., & Chen, R. 2022, ApJ, 933, 109